ISSN (Print) 1226-1750
ISSN (Online) 2233-6656
Journal of Magnetics 22(3), 450-462 (2017) https://doi.org/10.4283/JMAG.2017.22.3.450

Effect of Neodymium on the Magnetic and Dielectric Properties of Nickel-cobalt Ferrite

Basharat Want*, Rubiya Samad, and Mehraj ud Din Rather

Solid State Research Lab, Department of Physics, University of Kashmir, Srinagar-190006, India

(Received 23 March 2017, Received in final form 19 June 2017, Accepted 20 June 2017)

We investigate the effect of Nd doping on the magnetic and dielectric properties of nickel-cobalt ferrite. The samples were synthesized by sol-gel method and structural phase was determined by powder X-ray diffraction technique. X-ray diffraction studies reveal that the cubic spinel structure with space group Fd-3m is maintained for all the compositions. Doping with Nd atoms modified both the magnetic and dielectric properties of nickel-cobalt ferrite. A decrease in saturation magnetization and effective magnetic moment per atomic site is observed with increase in neodymium concentration. The doping of Nd into the Ni-Co ferrite lattice results in enhancement of coercivity and reduction of Curie temperature. The dielectric studies showed an increase in dielectric constant and decrease in loss tangent with the increase in Nd concentration. The frequency dependent dielectric measurements at room temperature were observed to obey the modified Debye model with a relaxation time of the order of 10^{-4} s and spreading factor in the range 0.47-0.69. The observed resonance relaxation peaks shift towards lower temperature with increase in Nd concentration.

Keywords : Spinel ferrites, Rare-earth, Hopkinson peak, Debye model, ac conductivity.

1. Introduction

Spinel ferrites constitute an important group of magnetic materials for technological applications such as electronics, opto-electronics, magnetic, magneto-electronics and electrochemical sciences [1-5]. Among spinel ferrites, nickel and cobalt ferrites have attracted scientific community for extra ordinary applications [6-8]. The incorporation of rare-earths in spinel ferrites induces strain in the lattice and tunes electrical as well as magnetic properties [9-20]. Among rare earths, Neodymium (Nd^{3+}) ions are suitable candidates to control various magnetic parameters for developing technologically important materials. The B-site preference of Neodymium in spinel ferrite produces significant changes in the lattice. The substitution of Nd^{3+} ions (3.64 μ_B) for Fe^{3+} (5 μ_B) alters magnetic properties similar to that of non-magnetic substitution [21]. To engineer the functional materials based on ferrites, doping with different rare-earth (RE) ions has proved to be a versatile way to tune their desirable structure and physical properties [22]. The properties of ferrites are also dependent on synthesis technique, microstructure and conditions employed for fabrication [23, 24]. The sol-gel auto combustion processes provide a possibility to control stoichiometry as well as size distribution of nanoparticles [25]. The structural, electrical and magnetic properties of spinel ferrites depend upon substitution of Fe ions by RE ions. The various properties of RE doped ferrites are a consequence of the incorporation of the rare earth atoms into the lattice, which results in a dramatic change in the spin coupling. The magnetic properties of such compounds are not only tailored by Fe-Fe interaction (3d electrons), but also by RE-Fe interaction [26-29].

In the present work, an attempt has been made to prepare a different spinel ferrite system $Ni_{0.9}Co_{0.1}Nd_yFe_{2-y}O_4$ (with $y = 0.0$, 0.1, 0.2, 0.3) by sol gel auto combustion technique. The effect of neodymium doping on structural, dielectric and magnetic properties of $Ni_{0.9}Co_{0.1}Nd_yFe_{2-y}O_4$ were studied. Substitution of Nd results in a high value of coercivity, and lowering of the curie temperature due to favourable $Fe^{2+} \leftrightarrow Fe^{3+}$ interactions. Substitution of Nd also results in low value of saturation magnetization. The observed decrease in net magnetization and a decrease in Curie temperature T_c with the increase in Nd content make these ferrites suitable for microwave devices operating at L, S and C bands. There may be good reasons to select a

©The Korean Magnetics Society. All rights reserved.
*Corresponding author: Tel: +911942420078
Fax: +911942423705, e-mail: bawant@kashmiruniversity.ac.in

© 2017 Journal of Magnetics

relatively low M_s and low curie temperature for microwave devices. First is the demagnetization field, the materials with low M_s has high demagnetization filed. In addition, one must consider the temperature dependence of the demagnetizing field which parallels the temperature dependence of M_s and thus produces a variation of the internal biasing field with temperature [30]. For a narrow linewidth material and for small values of p ($p = M_s/H_{z0}$, normalized saturation magnetization), the initial magnetic loss is low and decreases with p. This effect is known as low filed loss. This condition is achieved in materials with low saturation magnetization. It is quite troublesome at frequencies below 1 GHz because the saturation magnetization of the material cannot be made arbitrarily low. Therefore, this condition can be achieved in the frequency range from 1 GHz to few GHz that in the L, S and C bands. Magnetic loss in low M_s material can be expected to be small, so that dielectric loss may be contributing to the insertion loss of the devices as reported in literature [31]. The observed results and the effect of partial substitution of Fe by Nd on the electrical and dielectric properties are presented in this paper.

2. Materials and Method

The samples of the series $Ni_{0.9}Co_{0.1}Nd_yFe_{2-y}O_4$ (with y = 0.0, 0.1, 0.2, 0.3) were prepared by glycine-nitrate auto combustion route. The glycine, cobalt nitrate, neodymium nitrate, and ferric nitrate were used as starting materials. The ratio of metal nitrate to glycine was taken as 1:3. Reaction procedure was carried out in air atmosphere. The metal nitrates were dissolved together in a minimum amount of double-distilled water to get a clear solution. An aqueous solution of glycine was mixed with metal nitrate solution. Ammonium solution was added until pH reaches 6.5. The mixed solution was kept on a hot plate with continuous stirring at 80ºC. During evaporation, the solution became viscous and finally formed viscous brown gel. After a few minutes, the gel automatically ignited and burnt with glowing flints. The decomposition reaction does not stop before the whole glycine complex was consumed. The auto-ignition was completed within one minute, yielding the brown coloured ashes termed as precursor. The powder after completion of grinding process was then pre-sintered at 700ºC in a furnace for 5 hours, followed by furnace cooling. These pre-sintered samples were then pressed into pellets and toroidal rings using (3-5 wt.%) polyvinyl alcohol as a binder. The samples were finally sintered at 950ºC for 7 hours in an air atmosphere.

The XRD data of the synthesized samples were collected on the D8 Advance Bruker X-ray diffractometer with CuKα ($\lambda = 1.5406$ Å) radiation. The magnetic measurements were carried out by using a vibrating sample magnetometer (MicroSense EZ9 VSM, USA). For measurements of permeability, the sintered toroidal samples were wound with thin laminated copper wire. Inductance of the toroidal samples was measured using an impedance analyzer (Precision Component Analyzer, 6400B, Wayne Kerr electronics, UK) as a function of temperature and frequency. Initial permeability was calculated using the relation $\mu' = L/L_0$ [32, 33], where L is the measured inductance of the sample and L_0 is the air core inductance calculated using the dimensions of the coil. The dielectric measurements were carried out in the frequency range 20 Hz-3 MHz and over a temperature range 280 K-600 K.

3. Results and Discussion

3.1. XRD analysis

To investigate the structural parameters of $Ni_{0.9}Co_{0.1}Nd_yFe_{2-y}O_4$ (with $y = 0.0$, 0.1, 0.2, 0.3), Rietveld refinement of experimental XRD pattern of all samples was carried out using the FullProf suite software package [34, 35]. The XRD patterns of all the samples could be refined using the Fd-3m space group [36]. The X-ray diffraction patterns along with Rietveld refined data of all the samples of $Ni_{0.9}Co_{0.1}Nd_yFe_{2-y}O_4$ (with $y = 0.0$, 0.1, 0.2, 0.3) are shown in Fig. 1. The peaks in the diffraction pattern have been indexed.

The refined XRD patterns provide clear evidence of ferrite phase formation and confirm the cubic structure with Fd-3m space group in all the samples. The refined XRD patterns show that the neodymium doped samples contain $NdFeO_3$ (iron neodymium oxide) as secondary phase [37]. The percentage of the secondary phase increases with increasing neodymium concentration as given in Table 1. The secondary phase appears due to high reactivity of Fe^{3+}ions with rare-earth ions [38]. The Nd^{3+} ions are located at the grain boundaries instead of spinel lattice and form secondary phases as reported in literature for other rare-earth doped spinel ferrites [39, 40]. The presence of rare earth ions also inhibits grain growth as reported in the literature [39-41].

All the refined parameters obtained from Rietveld refinement are tabulated in Table 1, where R_b is Bragg factor and R_f is the crystallographic factor. The low values of χ^2 (goodness of fit) observed, confirm the high degree of refinement. The lattice constant 'a' increases slightly for $y = 0.1$ due to replacement of the smaller sized Fe^{3+} ions (0.64 Å) by larger Nd^{3+} ions (0.983 Å) causing dilation of the host spinel lattice. The decrease in lattice

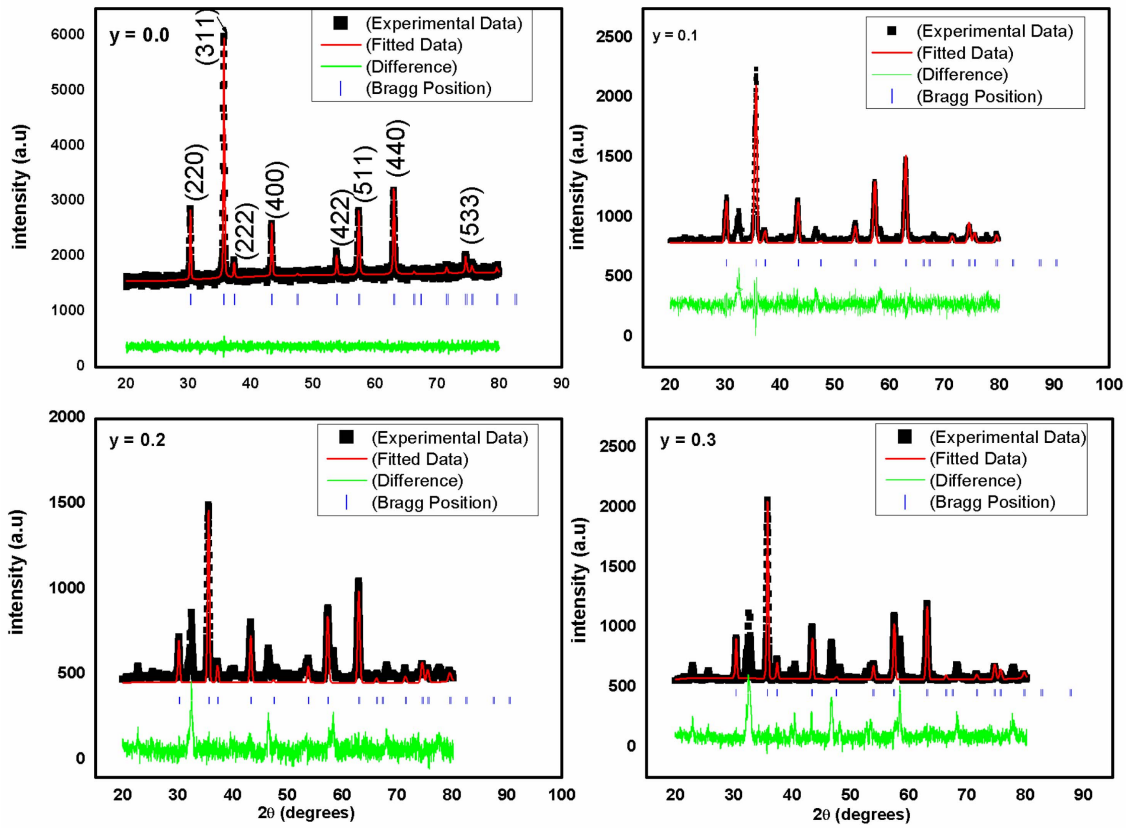

Fig. 1. (Color online) The observed, calculated, and difference Rietveld refined XRD patterns using FullPROF program for $Ni_{0.9}Co_{0.1}Nd_yFe_{2-y}O_4$ (with y = 0.0, 0.1, 0.2, 0.3).

Table 1. Rietveld agreement factors, lattice constant, and unit cell volume of $Ni_{0.9}Co_{0.1}Nd_yFe_{2-y}O_4$ (with y = 0.0, 0.1, 0.2, 0.3).

Y	a (Å)	V (Å^3)	D (g/cm^3)	χ^2	R_b	R_f	$NdFeO_3$
0.0	8.3435	580.82	5.3	1.03	4.36	4.35	-
0.1	8.3521	582.74	5.545	1.69	8.86	8.76	2.6 %
0.2	8.3403	580.14	5.782	2.44	16.6	16.1	5.2 %
0.3	8.3398	580.03	5.751	5.46	30.2	19.7	6.5 %

parameters for samples ($y > 0.1$) results due to compression of spinel lattice by the higher percentage of secondary phase [42, 43]. In case of rare-earth doping, the nucleation of orthoferrite phase in the intergranular interstices hinders grain growth, whereas it practically promotes densification [44] as evident from Table 1 that density increases with Nd^{3+} ions.

3.2. Magnetic Properties

Magnetic hysteresis loops recorded at room temperature for all samples of $Ni_{0.9}Co_{0.1}Nd_yFe_{2-y}O_4$ (with y = 0.0, 0.1, 0.2, 0.3) are shown in Fig. 2. From the hysteresis loops, the magnetic parameters have been calculated and are given in Table 2.

The saturation magnetization decreases with the increase in neodymium concentration. This is attributed to the fact that lesser magnetic moment Nd^{3+} ions (3.64 μ_B) replace higher magnetic moment Fe^{3+} ions (5 μ_B). In addition, the presence of antiferromagnetic intermediate phase ($NdFeO_3$) is also responsible for the reduction in saturation magnetization [45]. The magnetic moment (n_B) per formula unit in Bohr magneton (μ_B) was calculated by using the relation [46, 47].

$$n_B = \frac{M.W \times M_s}{5585}$$

Using the calculated magnetic moments, Yafet-Kittel (Y-K) angles were studied to see the spin arrangement in the prepared ferrite systems using the relation [46, 48, 49],

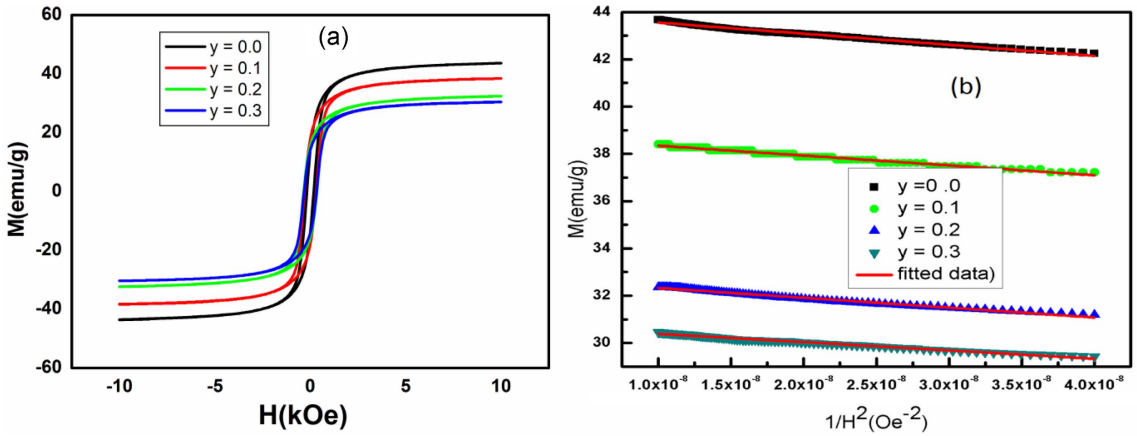

Fig. 2. (Color online) (a) Magnetic hysteresis loop of $Ni_{0.9}Co_{0.1}Nd_yFe_{2-y}O_4$ (with y = 0.0, 0.1, 0.2, 0.3) and (b) plot of M vs $1/H^2$.

$$Cos\,\theta_{Y-K} = \frac{n_B + 5(1-x)}{7+x},$$

where x represents the composition of doping ion. The Y–K angle increases with increase in Nd^{3+} concentration, owing to triangular spin arrangement of ions [50]. Magneto-crystalline anisotropy constant K_1 have been calculated from the "Law of Approach (LA)" analysis. LA describes the dependence of magnetization M on the applied magnetic field $H >> H_c$. The magnetization near the saturation M_s can be written as [51, 52]

$$M = M_s\left[1 - \frac{b}{H^2}\right]$$

Here $b = \frac{8}{105} \times \frac{K_1^2}{\mu_0^2 M_s^2}$, M is the magnetization, H is the applied magnetic field, M_s is the saturation magnetization, $\mu_0 = 4\pi \times 10^{-7}$ H/m is the permeability of the free space; K_1 is the cubic anisotropy constant. The numerical coefficient 8/105 applies to cubic anisotropy of random polycrystalline samples. Therefore, M_s and K_1 are the only fitting parameters in above equation. Experimental data [M-H curve] at high field (> 1 T) are fitted to above equation for the present series. Typical fitting curve to LA is shown in Fig. 2 for the samples $Ni_{0.9}Co_{0.1}Nd_yFe_{2-y}O_4$ (with $y = 0.0$, 0.1, 0.2, 0.3). The values of M_s and b are obtained from fitting and magneto-crystalline anisotropy constant (K_1) was calculated using the below equation [53]

$$K = \mu_0 M_s \sqrt{\frac{105b}{8}}$$

The magnetocrystalline anisotropy of pure Nickel-cobalt ferrite is primarily due to the presence of Co^{2+} ions on the octahedral sites (B-sites) of the spinel structure. The crystal field is not capable of removing the orbital degeneracy of Co^{2+} at the octahedral sites, so that the orbital magnetic moment is not quenched and hence there is strong spin-orbit coupling (L-S coupling) which produces magneto-crystalline anisotropy energy (MAE) [54]. The values of K_1 decrease with the increase in Nd^{3+} concentration which is due to decrease of the occupancy of Co^{2+} ions at the B-sites as reported by other researchers for rare-earth doped cobalt ferrite [53]. The calculated remanence ratio (M_R/M_S) lies in the range of 0.32 to 0.48, confirming multi-domain structure [55].

3.3. Temperature dependent permeability measurement

In order to determine the Curie temperature, the permeability (μ') was plotted against temperature at a constant frequency of 100 Hz. The increase in μ' with Nd substitution can be attributed to the increase in density consistent with rietveld studies [55]. In addition, the

Table 2. Magnetic parameters of $Ni_{0.9}Co_{0.1}Nd_yFe_{2-y}O_4$ (y = 0.0, 0.1, 0.2, 0.3).

y	M_S (emu/g)	M_r (emu/g)	Y-K angles	H_C (Oe)	M_r/M_s	$K \times 10^{-1}$(j/m^3)	n_B	T_c (°C)
0.0	43.65	14.02	12.58	178.13	0.32	2.07	1.83	620
0.1	38.38	17.9	29.63	307.32	0.47	1.829	1.67	575
0.2	32.39	15.64	40.66	347.16	0.48	1.68	1.46	565
0.3	30.81	13.99	47.49	331.82	0.45	1.49	1.43	560

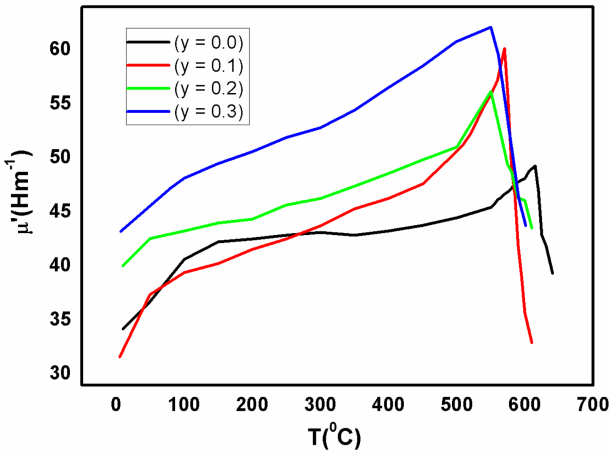

Fig. 3. (Color online) Variation of permeability with temperature for $Ni_{0.9}Co_{0.1}Nd_yFe_{2-y}O_4$ (with y = 0.0, 0.1, 0.2, 0.3)

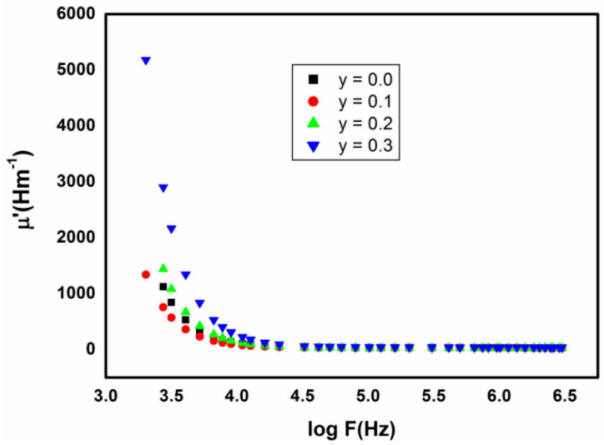

Fig. 4. (Color online) Variation of permeability with frequency for $Ni_{0.9}Co_{0.1}Nd_yFe_{2-y}O_4$ (with y = 0.0, 0.1, 0.2, 0.3)

movement of domain walls determines the value of μ' which is temperature dependent. Any increase in their number with increasing temperature would result in an increase in the initial permeability. The maximum value of μ' just below T_C is a manifestation of the Hopkinson peak attributed to the minimization of magneto-crystalline anisotropy energy with temperature [56, 57]. Beyond this peak, there is a sharp fall in μ' indicating T_C. The sharp fall of μ' at T_C indicates the degree of homogeneity in sample composition [58]. The obtained values of T_C from permeability measurements decrease with increase in Nd concentration. This decrease is due to replacement of Fe^{3+} ions by Nd^{3+} ions, which in turn weakens the super exchange interaction [59, 60].

3.4. Frequency dependent permeability measurements

The variations in initial permeability as a function of frequency in the range of 1 kHz-3 MHz is shown in Fig. 4. The initial permeability falls rapidly with increase in frequency upto 10 kHz and then remains fairly constant. This reflects that no structural relaxations or resonances took place in the observed frequency spectra [61]. The initial permeability in ferrites is due to domain wall displacement and remains constant with frequency as long as there is no phase lag between the applied field and the domain wall displacement [62]. The fairly constant values of μ' over a large frequency range show the compositional stability and quality of the ferrites prepared by the sol gel method [58]. From Table 2, it is evident that with the increase in Nd concentration permeability increases. The introduction of Nd^{3+} cations in the Ni-Co spinel lattice decreases the magneto-crystalline anisotropy, thereby densifies the ceramics and also increases the average particle size [63]. Thus, the domain wall oscillations are facilitated and their contribution to the permeability spectrum is enhanced as already reported for rare-earth doped Ni-Co ferrite [64]. A similar increase in initial permeability has been reported by other researchers with the addition of non-magnetic ion in doped spinel ferrite [65, 66]. The observed variations in initial permeability may be due to micro-structural parameters like average grain size and porosity [67].

3.5. Dielectric spectroscopy

3.5.1. Effect of frequency on the dielectric constant, dielectric loss and ac conductivity

The variation in real part of dielectric constant with frequency measured at room temperature (300 K) for $Ni_{0.9}Co_{0.1}Nd_yFe_{2-y}O_4$ (y = 0.0, 0.1, 0.2, 0.3) in the frequency range of 20 Hz-3 MHz is shown in Fig. 5. The dielectric constant sharply decreases with frequency (upto 1 kHz). At higher frequencies, dielectric constant decreases slowly and becomes almost constant (up to 3 MHz). The frequency dependence of dielectric constant is the characteristic of the usual dielectric dispersion. The dielectric dispersion observed can be explained by the contributions from various sources of polarizations [68]. The higher value of ε' at lower frequencies is attributed to the contributions from various polarizations such as ionic, space charge, and interface. The lower value of ε' at higher frequencies is due to the inability of the electric dipoles to be in pace with the frequency of applied electric field. Thus, the dielectric dispersion arising in the lower frequency region is associated with the interfacial polarization, because the atomic and electronic contribution to polarization remains unchanged at these frequencies [69]. Since more than one ion (O^{2-}, Fe^{3+}, Co^{2+}, Ni^{2+} and Nd^{3+} ions) contrib-

utes to the relaxation process, the data were fitted to the modified Debye's function [70].

$$\varepsilon' = \varepsilon_\infty' + \frac{\varepsilon_o' - \varepsilon_\infty'}{1 + (\omega\tau)^{2(1-\alpha')}}$$

Where ε' is the real part of the dielectric constant, ε_∞' is the dielectric constant at 3 MHz, ε_o' is the dielectric constant at 20 Hz, ω is the angular frequency, τ is the mean relaxation time, and α' is the spreading factor of the actual relaxation times about the mean value. The experimental data is in close agreement with the calculated data indicating the validity of modified Debye's function with the possibility of more than one ion contribution to the relaxation process. The dielectric constant attains maximum value at $y = 0.2$, and decreases thereafter, consistent with earlier studies of rare earth doped nickel and cobalt ferrites [70, 71]. As reported by Charalampos Stergiou, R^{3+} enters the spinel lattice, their large sizes create expansion and distortion of the unit cell [64]. Therefore, cation vacancies appear in order to accommodate these crystal modifications. The coexistence of the trivalent rare earth cations with the associated vacancies forms electric dipoles, which rotate under the influence of the applied ac electric field. The induced electric dipoles, in combination with the higher density of the rare earth substituted compounds, enhance the dielectric polarization of the materials and their permittivity. However, for $y = 0.3$, the decrease in ε' might be associated with the segregation ofhigher percentage of $NdFeO_3$ at the grain boundaries diminishes the Nd^{3+} cations that take place in the described dipole generation mechanism and compromises the polarization enhancement [64, 72, 73]. Therefore, due to the inclusion of higher percentage of impurity phase the dielectric constant decreases in comparison to pure nickel-cobalt ferrite.

The variation of dielectric loss (tanδ) with frequency at room temperatures is shown in Fig. 6. A maxima is observed in tanδ versus frequency curves in $Ni_{0.9}Co_{0.1}Nd_yFe_{2-y}O_4$ (with $y = 0.0$, 0.1, 0.2, 0.3). Iwauchi gave a qualitative explanation for the occurrence of the maxima in these curves [74]. The peak is observed when the electrons hopping frequency between Fe^{3+} and Fe^{2+} are in resonance with that of the frequency of applied electric field. The condition for the maximum tanδ of a material is $\omega\tau = 1$ [75]. The tanδ decreases rapidly in the low-frequency region, whereas a slight decrease is observed in central region and it becomes almost independent of frequency in higher frequency region. In the low-fre-

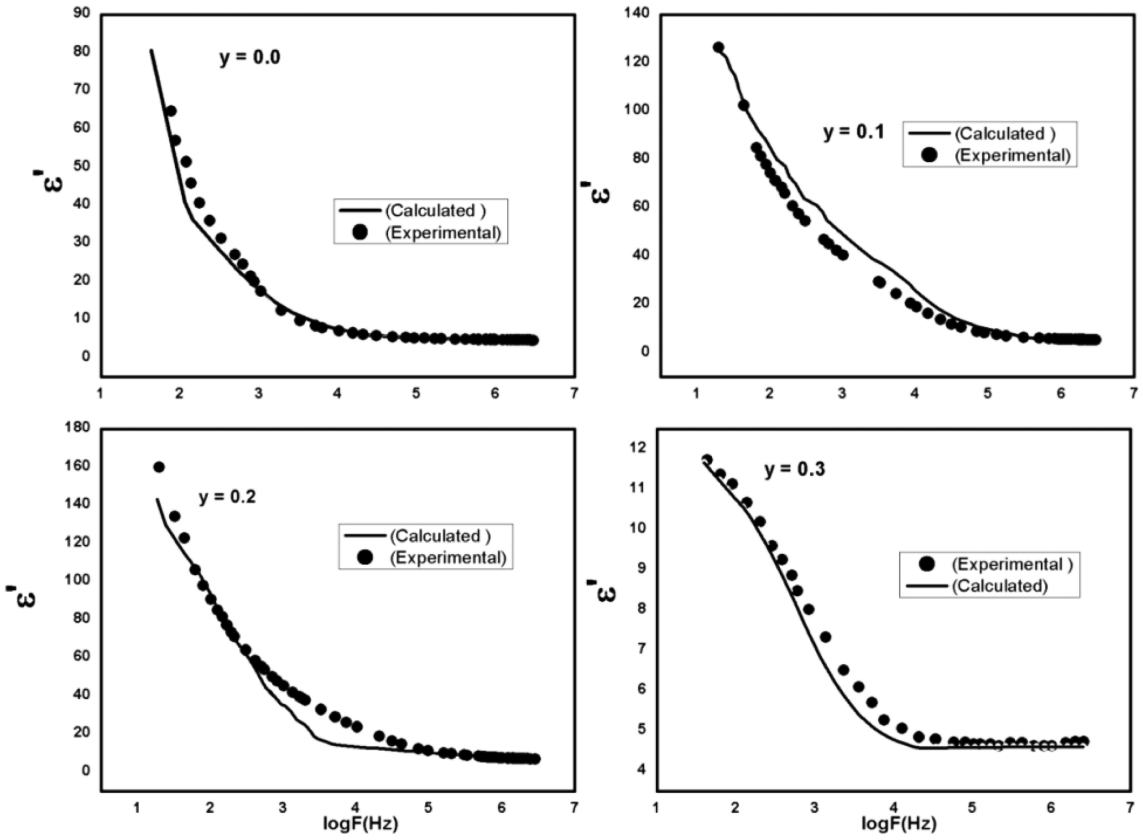

Fig. 5. The dielectric constant dispersion profiles of $Ni_{0.9}Co_{0.1}Nd_yFe_{2-y}O_4$ (with y = 0.0, 0.1, 0.2, 0.3).

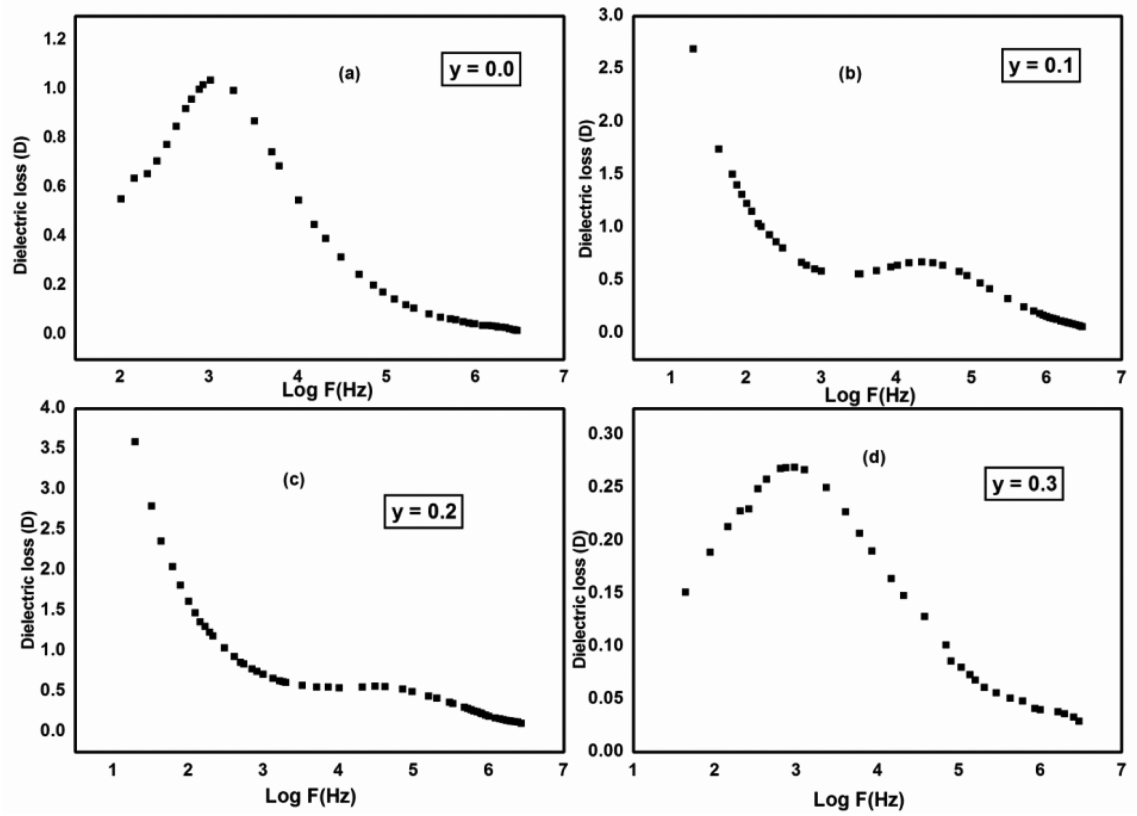

Fig. 6. Variation of dielectric loss with frequency for $Ni_{0.9}Co_{0.1}Nd_yFe_{2-y}O_4$ (with $y = 0.0$, 0.1, 0.2, 0.3).

quency region, the conductivity of grain boundary is very low and more energy is required for the exchange of electrons between Fe^{2+} and Fe^{3+} ions, resulting in high dielectric loss. In high-frequency region, there is high conductivity between grains, due to which a small energy is required for exchange of electrons between the Fe^{2+} and Fe^{3+} ions at the octahedral site [76, 77].

The ac conductivity (σ_{ac}) vs frequency was plotted at room temperature for $Ni_{0.9}Co_{0.1}Nd_yFe_{2-y}O_4$ (with $y = 0.0$, 0.1, 0.2, 0.3) as shown in Fig. 7. In the lower frequency region, a short dc plateau (frequency independent plateau) is observed, however frequency dependent conductivity was obtained in higher frequency region. The observed conductivity can be explained using jump relaxation model [78]. The frequency independent region at low- frequency is ascribed to the long range translational motion of ions contributing to dc conductivity. Funke explained the observed frequency independent dc conductivity behaviour in the jump relaxation model [78]. The conductivity at low-frequency region is correlated with the successful hopping between neighbouring vacant sites. These successive jumps result in long-range translational motion of ions that contribute to dc conductivity. The highest conductivity was found in case of $y = 0.2$, which might be associated with the partial substitution of Nd and secondary phase formation.

The frequency dependent ac conductivity of $Ni_{0.9}Co_{0.1}Nd_yFe_{2-y}O_4$ (with y = 0.0, 0.1, 0.2, 0.3) obeys Jonscher's power law of the form [79]

$$\sigma(\omega) = \sigma(0) + A\omega^n$$

where $\sigma(\omega)$ is the total conductivity, $\sigma(0)$ is the frequency

Table 3. Dielectric parameters of $Ni_{0.9}Co_{0.1}Nd_yFe_{2-y}O_4$ (with $y = 0.0$, 0.1, 0.2, 0.3).

y	ε (1 kHz)	τ (sec)	α	tanδ (D)	σ_{ac} ($\Omega^{-1}m^{-1}$)	E_a (500 kHz)
0.0	17.49	9.43×10^{-4}	0.69	1.038	1.06×10^{-6}	0.34 eV
0.1	40.32	0.45×10^{-4}	0.65	0.585	1.32×10^{-6}	0.397 eV
0.2	45.38	0.32×10^{-4}	0.58	0.709	1.8×10^{-6}	0.26 eV
0.3	7.9	1.04×10^{-3}	0.47	0.269	1.3×10^{-7}	0.21 eV

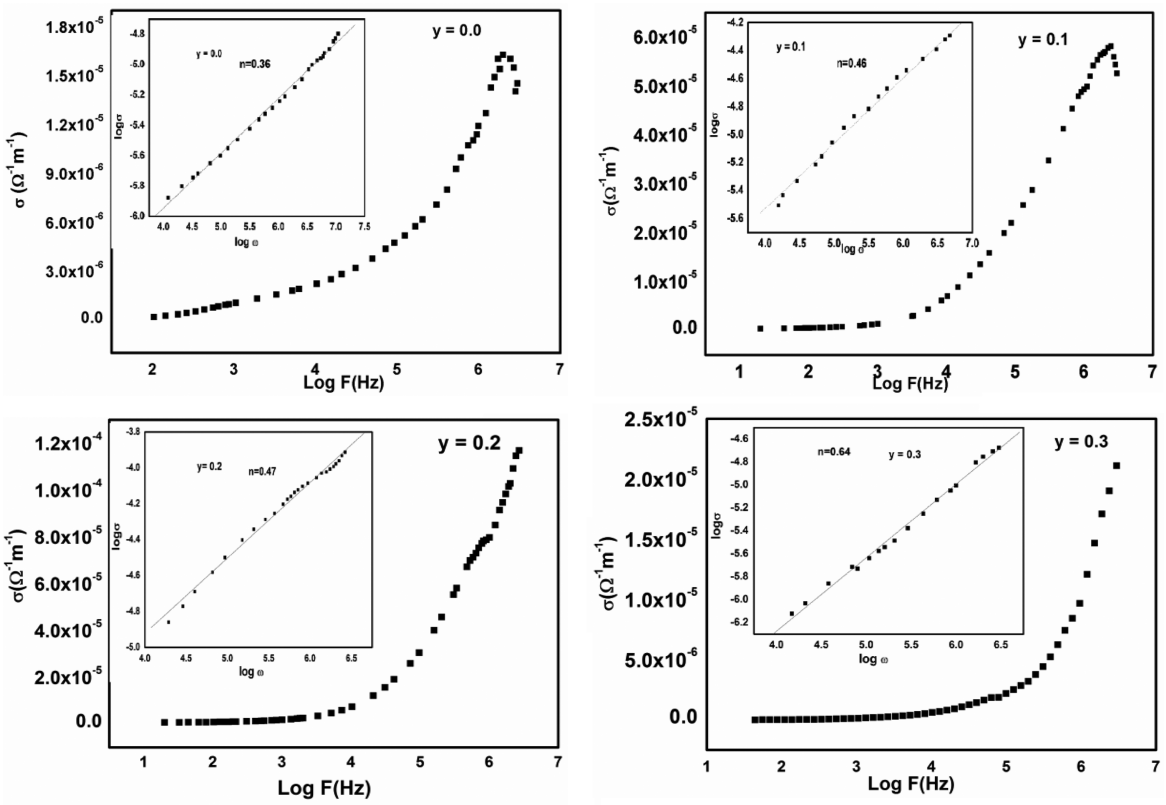

Fig. 7. Variation of ac conductivity with frequencies and inset plot Log σ_{ac} versus log ω for $Ni_{0.9}Co_{0.1}Nd_yFe_{2-y}O_4$ (with y = 0.0, 0.1, 0.2, 0.3).

independent conductivity, and the coefficient A and exponent n ($0 < n < 1$) are temperature and material intrinsic property dependent constants. The term $A\omega^n$ contains the ac dependence and characterizes all dispersion phenomena in higher frequency region ($f > 1$ kHz). The value of n defines the motion of charge carriers, either translational or localized. If value of n is $n < 1$, the motion is translational, and if value of n is $n > 1$, the motion is localized [80]. Different hopping mechanisms have been reported by various researchers which predicted different temperature and frequency dependence on exponent n. As shown in inset of Fig. 7, the numerical values of n obtained are below 1, and hence it is concluded that the conduction arises primarily due to the short-range translational motion assisted by both large and small polaron hopping mechanisms.

3.5.2. Effect of temperature on the dielectric constant, dielectric loss and ac conductivity

The temperature dependence of dielectric constant for $Ni_{0.9}Co_{0.1}Nd_yFe_{2-y}O_4$ (with $y = 0.0$, 0.1, 0.2, 0.3) at different frequencies is shown in Fig.8. The dielectric constant is nearly temperature independent in the lower temperature range, while dielectric constant increases with temperature for all frequencies. The thermal energy supplied to charge carriers enhances the mobility of these carriers, which results in increase in hopping rate. However, thermal energy supplied at lower temperature is not enough to increase the mobility of the charge carriers. Therefore, dielectric polarization increases at higher temperature, which leads to increase in dielectric constant [81].

The variation of dielectric loss with temperature at various frequencies is shown in Fig. 9. The dielectric loss first increases with temperature, attains the maxima and then decreases. The increase in dielectric loss with temperature might be associated with increasing lattice vibrations and formation of some phonons which interact with the charge carriers and give rise to electron phonon scattering. The resonance relaxation peaks can be clearly seen, and they shift towards higher temperature with increasing frequency. The observed shift of the relaxation peak is a clear indication of the thermally activated relaxation process, which is the typical of relaxation losses in dielectric materials [82, 83]. The shift of relaxation peaks is often ascribed to the increase in hopping rate of charge carriers. The relaxation time s is correlated with the jumping probability per unit time "p" as: $\tau = 1/2P$ or

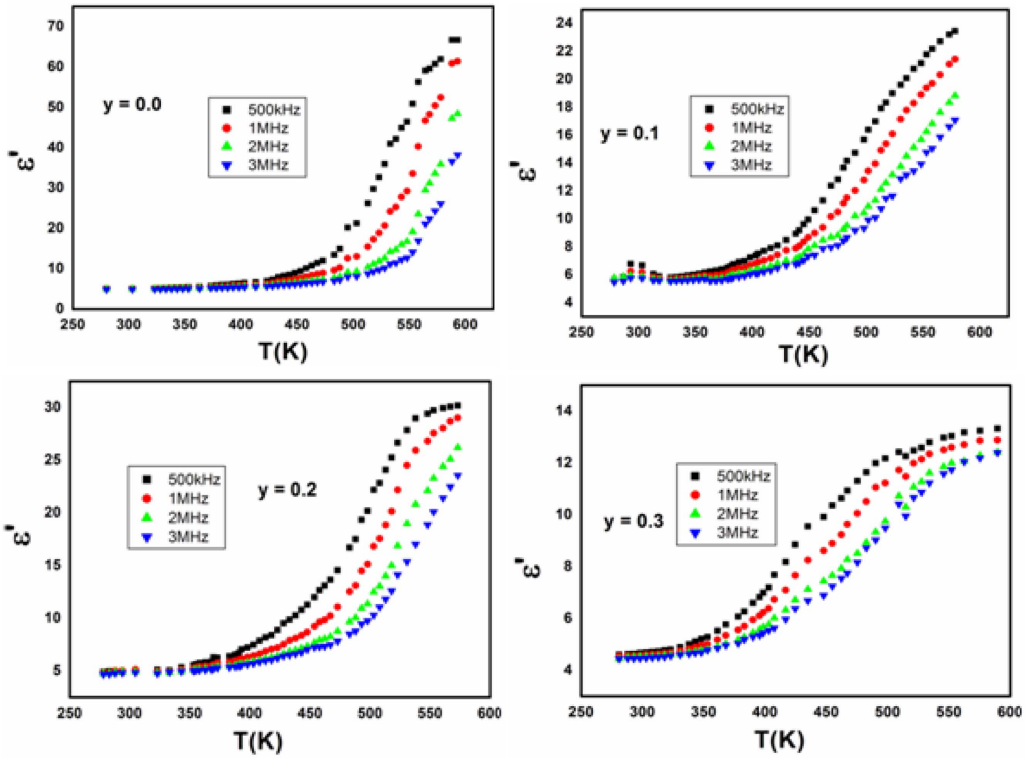

Fig. 8. (Color online) Variation of dielectric constant with temperature for $Ni_{0.9}Co_{0.1}Nd_yFe_{2-y}O_4$ (with $y = 0.0$, 0.1, 0.2, 0.3).

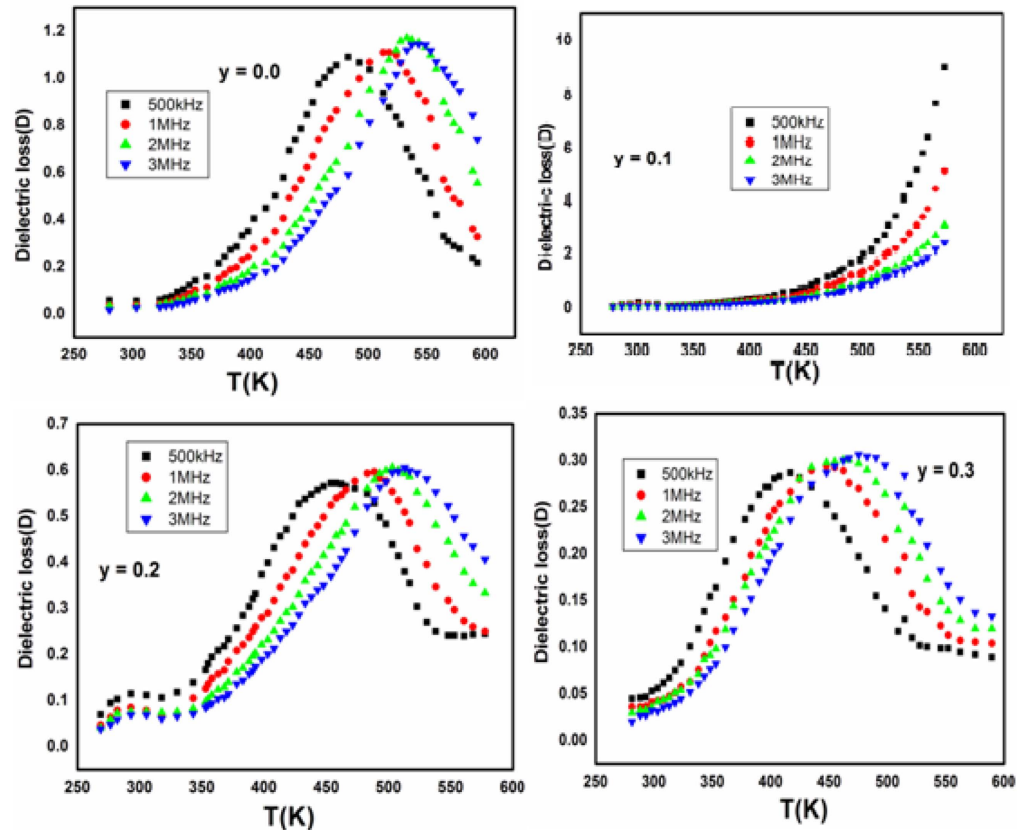

Fig. 9. (Color online) Variation of dielectric loss with temperature for $Ni_{0.9}Co_{0.1}Nd_yFe_{2-y}O_4$ (with $y = 0.0$, 0.1, 0.2, 0.3).

$\omega_{max} = 2P$. The shift of peaks to higher temperature with frequency indicates increase in the jumping probability per unit time 'P' with increasing frequency. However, the remarkable effect of Nd is manifested by the peak shift towards a lower temperature with the increase in *y*. This observation clearly indicates that jumping probability per unit time decreases as Nd^{3+} content in Ni-Co ferrite increases as reported in literature for other ferrites [84]. A completely different behaviour was found for $Ni_{0.9}Co_{0.1}$-$Nd_{0.1}Fe_{1.9}O_4$ where no loss peak is found and tanδ increases with temperature. This increase might be due to the easier motion of free charges at high temperature. Similar results are also reported in the literature [85].

Variation of ac conductivity (σ_{ac}) with temperature for the pure and Nd-substituted Ni-Co ferrite samples at various frequencies are shown in Fig. 10. The σ_{ac} increases with temperature for all selected frequencies and this increase is more prominent at higher frequencies. This increase in conductivity with temperature might be attributed to the increase in drift mobility of the charge carriers thereby enhancing their hopping rate [85]. In the high temperature region, higher magnitude of conductivity at higher frequencies is an expected result in view of strong frequency dependence under these conditions. At different frequencies, by the decrease in temperature, the electrical conductivity of the materials approaches each other in the lower temperature region. The variation in the conductivity indicates that the electrical conduction is a thermally activated process and is governed by the release of space charge [86].

Fig. 11 shows the variation of ac conductivity with inverse of temperature at different frequencies. The activation energy for different frequencies was estimated using Arrhenius relation

$$\sigma_{ac} = \sigma_o \exp\frac{-E_a}{k_B T}$$

Where σ_o is the prefactor, E_a the activation energy for charge conduction. The activation energies calculated from ac conductivity spectra in temperature range from 300 K-500 K at selected frequencies are given in Table 3. The activation energies decrease with the increase in Nd concentration. This can be interpreted and explained on the basis of increase in hopping pairs. The Nd^{3+} ions that substitute Fe^{3+} ions may have energy levels, which shift the Fe^{3+} energy levels towards Co^{2+}, or Ni^{2+} levels so that the hopping between Fe^{2+} and Fe^{3+} increases and thereby increases the conductivity. In present study, the decrease in activation energy with the increase in Nd^{3+} concentration supports the enhanced conductivity as also reported in literature [87]. The decrease in activation energy is ascribed to the redistribution of small sized cations. The

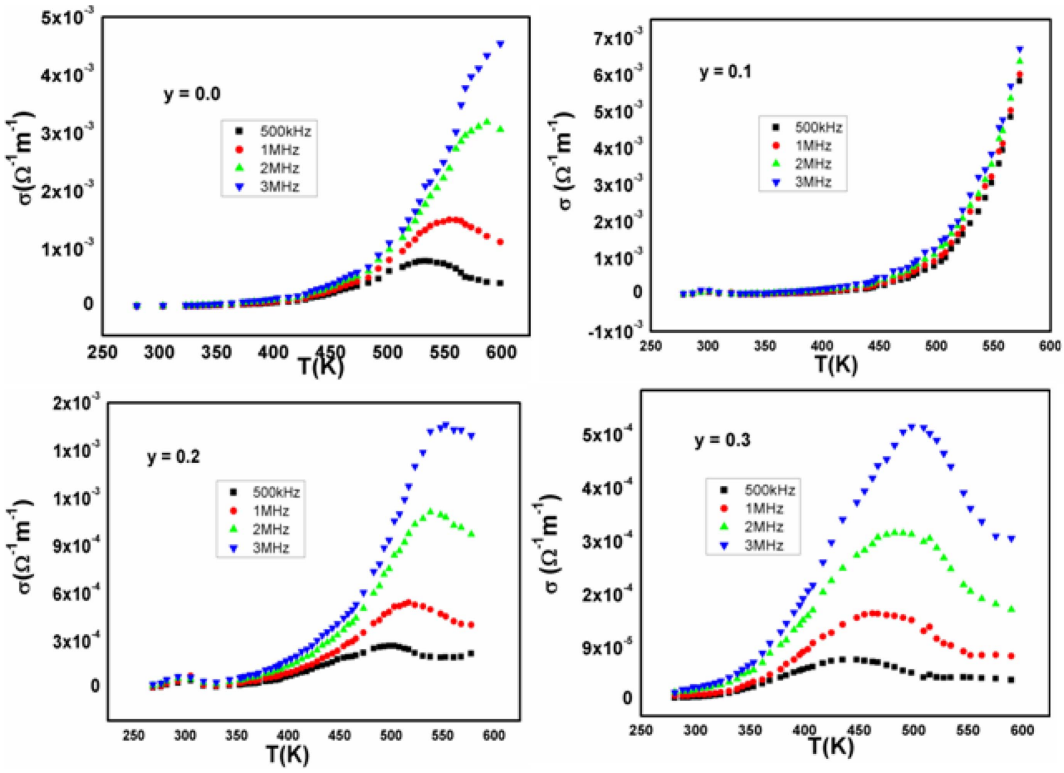

Fig. 10. (Color online) Variation of ac conductivity with temperature for $Ni_{0.9}Co_{0.1}Nd_yFe_{2-y}O_4$ (with $y = 0.0, 0.1, 0.2, 0.3$).

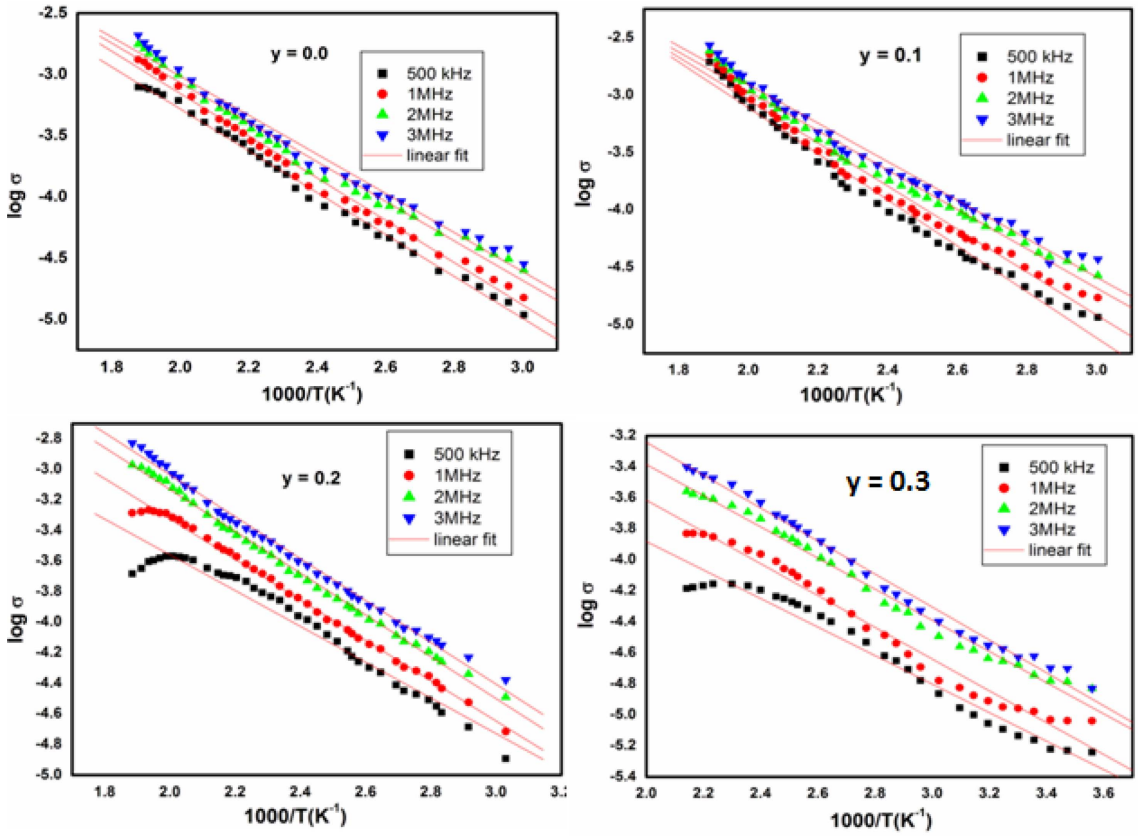

Fig. 11. (Color online) Variation of conductivity with inverse of temperature for $Ni_{0.9}Co_{0.1}Nd_yFe_{2-y}O_4$ (with y = 0.0, 0.1, 0.2, 0.3)

electrical conductivity of $Ni_{0.9}Co_{0.1}Nd_{0.3}Fe_{1.7}O_4$ is found to be less compared to $Ni_{0.9}$ $Co_{0.1}Nd_{0.2}Fe_{1.8}O_4$. Due to the non-incorporation of higher Nd^{3+} content in the Ni-Co ferrite, the transfer of Fe^{3+} ions from the tetrahedral sites to octahedral sites are limited. Also, owing to the formation of large number of $NdFeO_3$ secondary phase in $Ni_{0.9}Co_{0.1}Nd_{0.3}Fe_{1.7}O_4$, the number of Fe^{3+} ions decreases and ultimately $Fe^{2+} \leftrightarrow Fe^{3+}$ ion pairs. Since, the electrons hopping between $Fe^{2+} \leftrightarrow Fe^{3+}$ ions are responsible for electrical conduction; a decrease in $Fe^{2+} \leftrightarrow Fe^{3+}$ ion pairs decreases the electrons hopping and also electrical conductivity of $Ni_{0.9}Co_{0.1}Nd_{0.3}Fe_{1.7}O_4$.

4. Conclusion

Nd^{3+} substituted Ni-Co ferrite with chemical formula $Ni_{0.9}Co_{0.1}Nd_yFe_{2-y}O_4$ (y = 0.0, 0.1, 0.2, 0.3) was successfully synthesized by sol gel auto combustion method. The XRD pattern revealed that the cubic spinel structure is maintained as dominant phase for all compositions. Increase in lattice constant is observed due to replacement of the smaller Fe^{3+} ions with larger Nd^{3+} ions causing dilation of the host spinel lattice. The saturation magnetization is found to decrease with increase in Nd^{3+} content, while as Yeffit-Kittel angles increases with increase in Nd concentration, showing a triangular spin arrangement for present ferrite system. It is also observed that Curie temperature decreases with increase in the Nd concentration. The observed decrease in net magnetization and a decrease in Curie temperature T_c with the increase in Nd content make these ferrites suitable for microwave devices operating at L, S and C bands. The increase in permeability with increase in Nd content and its constant value over a large frequency range shows compositional stability. The frequency dependent behaviour of the dielectric constant at room temperature was explained by modified Debye model. The frequency dependent ac conductivity obeys Jonscher's power law, which reveals that the conduction arises mainly due to the short-range order translational hopping assisted by both large and small polaron hopping mechanisms.

Acknowledgment

One of the authors Rubiya Samad highly acknowledges Department of Science and Technology, Government of India for financial support vide reference no. SR/WOS-A/PM-1006/2015 under Women Scientist Scheme to carry

out this work. The authors are thankful to the authorities of the University of Kashmir for providing the vibrating sample magnetometer facility (MicroSense EZ9 VSM) to the Department of Physics under DST Govt. of India special package for sophisticated instrumentation.

References

[1] M. Sugimoto, J. Am. Cer. Soc. **82**, 269 (1999).
[2] S. Zahi, Mater. Des. **31**, 1848 (2010).
[3] Gu. Zhijun, Xu. Xiang, Guoli. Fan, and Feng. Li, J. Phys. Chem. C **112**, 18459 (2008).
[4] G. Hu, J. H. Choi, C. B. Eom, V. G. Harris, and Y. Suzuki, Rapid Communications Phys. Rev. B **62**, 779 (2000).
[5] Q. Song and Z. J. Zhang, J. Phys. Chem. B **110**, 11205 (2006).
[6] D. Carta, M. F. Casula, A. Falqui, D. Loche, G. Mountjoy, C. Sangregorio, and A. Corrias, J. Phys. Chem. C **113**, 8606 (2009).
[7] M. H. Sousa, F. A. Tourinho, J. Depeyrot, G. J. Silva, and Maria Cristina F. L. Lara, J. Phys. Chem. B **105**, 1168 (2001).
[8] B. G. Toksha, Sagar E. Shirsath, M. L. Mane, S. M. Patange, S. S. Jadhav, and K. M. Jadhav, J. Phys. Chem. C **115**, 20905 (2011).
[9] Qing Lin, Guangbai Yuan, Yun He, Liping Wang, Jianghui Dong, and Yang Yu, Mater. Des. **78**, 80 (2015).
[10] M. K. Shobana, Wonjong Nam, and HeemanChoe, J. Nanosci. Nanotechnol. **13**, 3535 (2013).
[11] J. P. Singh, H. Kumar, A. Singhal, N. Sarin, R. C. Srivastava, and K. H. Chae, Appl. Sci. Lett. **2**, 03 (2016).
[12] S. E. Jacobo, S. D. Uhalde, and H. R. Bertorello, J. Magn. Magn. Mater. **272**, 2253 (2004).
[13] G. Bulai, L. Diamandescu, I. Dumitru, S. Gurlui, M. Feder, and O. F. Caltun, J. Magn. Magn. Mater. **390**, 123 (2015).
[14] Z. Karimi, Y. Mohammadifar, H. Shokrollahi, ShKhamenehAs, GhYousefi, and L. Karimi, J. Magn. Magn. Mater. **361**, 150 (2014).
[15] S. R. Naik and A. V. Salker, J. Mater. Chem. **22**, 2740 (2012).
[16] K. K. Bharathi, J. A. Chelvane, and G. Markandeyulu, J. Magn. Magn. Mater. **32**, 3677 (2009).
[17] K. K. Bharathi, R. J. Tackett, C. E. Botez, C. V. Ramana, J. Appl. Phys. **109**, 07A510 (2011).
[18] N. Rezlescu and E. Rezlescu, Solid State Commun. **88**, 139 (1993).
[19] H. S. Aziz, S. Rasheed, R. Ali Khan, A. Rahim, J. Nisar, S. M. Shah, F. Iqbal, and A. R. Khan, RSC Adv. **6**, 6589 (2016).
[20] K. Kamala Bharathi, M. Noor-A-Alam, R. S. Vemuri, and C. V. Ramana, RSC Adv. **2**, 941 (2012).
[21] S. Amiri and H. Shokrollahi, J. Magn. Magn. Mater. **345**, 18 (2013).
[22] B. Zhou, Y. W. Zhang, C. S. Liao, C. H. Yan, L. Y. Chen, and S. Y. Wang, J. Magn. Magn. Mater. **280**, 327 (2004).
[23] S. Amiri and H. Shokrollahi, Mater. Sci. Eng., C **33**, 1 (2013).
[24] S. D. Bhame and P. A. Joy, J. Appl. Phys. **100**, 113911 (2006).
[25] D. H. Chen and X. R. He, Mater. Res. Bull. **36**, 1369 (2001).
[26] S. Chikazumi, New York, Oxford University Press, 1997.
[27] N. Rezlescu, E. Rezlescu, C. Pasnicu, and M. L Craus, J. Phys. Condens. Matter. **6**, 5707 (1994).
[28] T. J. Shindea, A. B. Gadkari, and P. N. Vasambekar, J. Alloys Compd. **513**, 80 (2012).
[29] K. K. Bharathi, J. A. Chelvaneb, and G. Markandeyulu, J. Magn. Magn. Mater. **321**, 3677 (2009).
[30] W. H. Von Aulock, "Temperature-compensated gyromagnetic device," U.S.A. Patent 3 030593A, 1962.
[31] W. H. Von Aulock, IEEE Trans. Magn. **2**, 251 (1966).
[32] C. Heck, Magnetic Materials and Their Applications, London: Butterworths (1974).
[33] S. H. Keluskar, R. B. Tangsali, G. K. Nail, and J. S. Budkuley, J. Magn. Magn. Mater. **305**, 296 (2006).
[34] J. Rodriguez-Carvaja, Physica B **192**, 55 (1993).
[35] R. Y. Young, The Rietveld Method, International Union of Crystallography Monographs on Crystallography, Oxford University Press, Oxford (1996).
[36] S. Carbonin, F. Martignago, G. Menegazzo, and A. Negro, Phys. Chem. Miner. **29**, 503 (2002).
[37] M. D. Luu, N. N. Dao, D. V. Nguyen, N. C. Pham, N. Vu and T. D. Doan, Adv. Nat. Sci.: Nanosci. Nanotechnol. **7**, 025015 (2016).
[38] A. B. Gadkari, T. J. Shinde, and P. N. Vasambekar, Mater. Chem. Phys. **114**, 505 (2009).
[39] N. Rezlescu and E. Rezlescu, J. Phys. IV France, **7**, C1-225 (1997).
[40] E. Ateia, M. A. Ahmed, and A. K. El-Aziz, J. Magn. Magn. Mater. **311**, 545 (2007).
[41] M. A. Ahmed, N. N. Okasha, and M. M. El-Sayed, Ceram. Inter. **33**, 49 (2007).
[42] J. Peng, M. Hojamberdiev, X. Yunhua, B. Cao, J. Wang, and W. J. Magn. Magn. Mater. **323**, 133 (2011).
[43] G. Dascalu, G. Pompilian, B. Chazallon, V. Nica, O. F. Caltun, S. Gurlui, and C. Focsa, Appl. Phys. A **110**, 915 (2013).
[44] C. Stergiou and G. Litsardakis, AIP Conference Proceedings **1627**, 117 (2014).
[45] I. Sosnowska, E. Steichele, and A. Hewat, Physica **136b**, 394 (1986).
[46] Y. Yafet and C. Kittel, Phys. Rev. **87**, 290 (1952).
[47] R. C. Kambale, P. A. Shaikh, S. S. Kamble, and Y. D. Kolekar, J. Alloys Compd. **478**, 599 (2009).
[48] V. G. Panicker, R. V. Upadhyay, S. N. Rao, and R. G. Kulkarni, J. Mater. Sci. Lett. **3**, 385 (1984).
[49] A. K. Nikumbh, A. V. Nagwade, G. S. Gugale, M. G. Chaskar, and P. P. Bakare, J. Mater. Sci. **37**, 637 (2002).

[50] W. Chen, W. Zhu, C. Ke, Z. Yang, L. Wang, X. F. Chen, and O. K. Tan, J. Alloys. Compd. **508**, 141 (2010).
[51] R. Grössinger, Phys. Status Solidi A **66**, 665 (1981).
[52] S. Chikazumi, Physics of Ferromagnetism, second ed., Oxford University Press, New York, 1997.
[53] L. Kumar and M. Kar, Ceramics International 38, 4771 (2012).
[54] B. D. Culity, Introduction to Magnetic Materials, Addision-Wesely, 1972.
[55] C. Sudakar, G. N. Subbanna, and T. R. N. Kutty, J. Magn. Magn. Mater. **263**, 253 (2003).
[56] D. Polder, Inst. Electron Eng. Part II, **97**, 246 (1950).
[57] G. Kumar, J. Chand, S. Verma, and M Singh, J. Phys. D: Appl. Phys. **42**, 155001 (2009).
[58] A. Globus and P. Duplex, IEEE Trans. Magn. Magn. **2**, 441 (1966).
[59] A. V. Jagadeesha, B. Rudraswamy, K. Sadhana, and K. Praveena, Materials Today: Proceedings **3**, 2178 (2016).
[60] K. Kamala Bharathi, G. Markandeyulu, and C. V. Ramana, J. Phys. Chem. C **115**, 554 (2011).
[61] S. M. Hoque, M. S. Ullah, F. A. Khan, M. A. Hakim, and D. K. Saha, Physica B: Condensed Matter **406**, 1799 (2011).
[62] A. K. Singh, T. C. Goel, R. G. Mendiratta, O. P. Thakur, and C. Prakash, J. Appl. Phys. **92**, 3872 (2002).
[63] C. Stergiou and G. Litsardakis, AIP Conference Proceedings **1627**, 117 (2014).
[64] C. Stergiou, J. Magn. Magn. Mater. **426**, 629 (2017).
[65] L. G. Van Uitert, J. Appl. Phys. **26**, 1289 (1955).
[66] A. K. M. AktherHossain and M. L. Rahman, J. Magn. Magn. Mater. **323**, 1954 (2011).
[67] J. Smit and H. P. J. Wijn, Philips Tech. Library (Netherlands) (1959) p. 150.
[68] A. Verma, O. P Thakur, C. Prakash, T. C. Goel, and R. G. Mendiratta, Mater. Sci. Eng. B **116**, 1 (2005).
[69] R. C. Kambale, P. A Shaikh, C. H. Bhosale, K. Y Rajpure, and Y. D. Kolekar, Smart Mater. Struct. **18**, 115028 (2009).
[70] K. Kamala Bharathi, G. Markandeyulu, and C. V. Ramana, J. Phys. Chem. C **115**, 554 (2011).
[71] K. Kamala Bharathi and C. V. Ramana, J. Mater. Res. **26**, 584 (2011).
[72] X. Ren and G. Xu, J. Magn. Magn. Mater. **354**, 44 (2014).
[73] N. Chen and M. Gu, Open J. Met. **2**, 37 (2012).
[74] K. Iwauchi, Jpn. J. Appl. Phys. **10**, 1520 (1971).
[75] Amarendra K. Singh, T. C. Goel, R. G. Mendiratta, and O. P. Thankur, J. Appl. Phys. **91**, 6626 (2002).
[76] P. V. Reddy and T. S. Rao, J. Less Common Metals **86**, 255 (1982).
[77] C. S. Narasimhan and C. S. Swamy, Phys. Stat. Sol. A **59**, 817 (1980).
[78] K. Funke, Prog. Solid St. Chem. **22**, 111 (1993).
[79] A. K. Jonscher, Nature **267**, 673 (1977).
[80] S. Kumari, N. Ortega, A. Kumar, S. P. Pavunny, J. W. Hubbard, C. Rinaldi, G. Srinivasan, J. F. Scott, and Ram S. Katiyar, J. Appl. Phys. **117**, 114102 (2015).
[81] Y. D. Kolekar, L. J. Sanchez, and C. V. Ramanaa, J. Appl. Phys. **115**, 144106 (2014).
[82] I. S. Zheludev, Physics of Crystalline Dielectrics: Electrical Properties, Plenum Press, New York (1971), Vol. 2, p. 517.
[83] M. C. Castro Jr., C. W. A. Paschoal, F. C. Snyder, and M. W. Lufaso, J. Appl. Phys. **104**, 104114 (2008).
[84] A. Schönhals and F. Kremer, Analysis of Dielectric Spectra in Broadband Dielectric Spectroscopy, in: F. Kremer, A. Schönhals (Eds.), Springer, Berlin, Heidelberg (2003) pp 59-98.
[85] Md. T. Rahman, M. Vargas, and C. V. Ramana, J. Alloys. Compd. **617**, 547 (2014).
[86] S. Chatterjee, P. K. Mahapatra, R. N. P. Choudhary, and A. K. Thakur, Phys. Status Solidi A **201**, 588 (2004).
[87] C. Murugesan and G. Chandrasekaran, RSC Adv. **5**, 73714 (2015).